

Supplementary material

**Table S1.** Proposed metadata attributes for spectroradiometric data for F retrieval grouped by metadata categories, with core attributes shaded in gray and justification for their inclusion in the F metadata set. Attributes or metadata categories that are not yet included in the SPECCHIO metadata model are indicated with an asterisk\*.

Attributes per Metadata Category	Justification
General	
Acquisition Time (UTC)	The acquisition time, in combination with the spatial position, defines the sun angle and is required for time series. UTC is a must for the integration of data across time zones and daylight savings.
File Name	Part of a unique file identification system, related to the name of a file produced by spectroradiometer control software.
Generic Target Properties	
Basic Target Type	A categorical variable defining the target type at a scale appropriate to the measurement support. Required for comparative studies selecting data via target types.
Site ID	Unique identifier of a sampling site, which may comprise several targets. Required to select all data for a single site or to group data by site for comparative studies.
Target Scale	A categorical variable indicating if measurements were taken at the leaf, single plant, or canopy level. Required for scale-dependent analysis.
Target Structure*	A representation of the target structure as a surface model or 3D point cloud to allow modeling of the direct/diffuse irradiance of the measurement support [1]. Requires optical properties of the target if a radiative transfer model is to be parametrized.
Target Description	A textual description of the target. Used to capture information not specified by the Basic Target Type. May be superseded by photos and physical measurements of the target structure.
Target ID	A unique identifier for a target within a site. Used to select a specific target of a site or group data by target for site-related studies.
Instrument	
Calibration Number	A unique number or alphanumeric value that specifies a set of calibration vectors (wavelengths, FWHMs, radiometric gains, and other variables pertaining to an instrument model <sup>1</sup> [2]) of a particular instrument.
Instrument Serial Number	A unique number of an instrument. Required to establish a link with the calibration data in conjunction with the calibration number.
Sensor/Instrument Type	A model identifier. Required for the selection of the correct instrument model <sup>1</sup> for that type of instrument.
Center Wavelengths	The center wavelengths of each spectral band. This information is critical for F retrieval.

<sup>1</sup> By instrument model, we refer to the concept of a software component that can execute forward and inverse simulations of the measurement process.

FWHMs or SRFs*	The per-band bandwidth as a scalar or spectral response function as a vector if not approximated by a Gaussian. Important parameter to quantify the smoothing influence on sharp absorption features in combination with the center wavelength. Required for instrument and data inter-comparisons [3].
Instrument Settings	
Automatic Dark Current Correction	A flag indicating whether the instrument implemented an automatic dark current correction and that the dark current signal is not explicitly available. Such implementations limit the information about the state of the instrument, likely leading to higher uncertainties.
Capturing Software Version	The software version should be part of the metadata generated by the instrument and may be indicative of changes in the acquisition of the spectroradiometric signal. Required for post-processing algorithms.
Gain/Offset	The radiometric gains and offsets applied during data capture. Required for radiometric calibration and parametrization of the instrument model.
Instrument Temperature	Required for monitoring and compensation of temperature effects via the instrument model [4,5].
Integration Time	The integration time applied during data capture. Required for radiometric calibration and parametrization of the instrument model in cases of nonlinearities [6].
Number of internal Scans	Governs the signal-to-noise ratio by taking internal averages. Important for noise analysis and optimization of instrument configuration.
Location	
Altitude	Required for radiative transfer modeling of the observed target, as the O <sub>2</sub> absorption band depths are a function of the altitude [7].
Latitude, Longitude	Required for solar angle calculations and data selection by spatial location.
Location Name	Required for text-based searches and automated report generation.
Optics	
FOV	Required for the measurement support calculation and for modeling of at-sensor radiance due to BRDF effects in combination with the selected FOV [8,9].
FOV Response Function*	Angularly resolved spectroradiometric sensitivity function of the FOV [10]. Required to weight the measurement support when modeling at-sensor radiances or to determine the radiometrically most contributing area of the target.
Sampling Geometry	
Beam Geometry	Defines the geometries of incoming and outgoing radiation [11]. Required for comparison of data [12].
Illumination Azimuth & Zenith	Required for radiative transfer modeling or for selection of data for certain solar geometries. Has an impact on the radiometric uncertainty of the irradiance measurement [13].
Measurement Support Area, Major/Minor Axis	The area of the projected field of view and the size of the axes of the elliptical footprint, calculated from FOV, sensor distance, and sensor zenith. Required for inter-comparisons between different setups and impact of target structure sizes [9].

Sensor Azimuth & Zenith	Required for measurement support calculations and BRDF modeling.
Sensor Distance	Required for measurement support calculations.
Environmental Conditions	
Air Pressure	Required for the modeling of altitude pressure effects [14] on the depth of O <sub>2</sub> absorption bands [15].
Ambient Temperature	Required for the study of the effect of environmental conditions on the photosynthetic apparatus [16].
Relative Humidity	
Soil Temperature*	
Water Content	
Cloud Cover	Percent of the hemisphere covered by clouds. May be useful to link with observed PAR or solar irradiance.
Wind Speed	Can be used to explain fluctuations in spectroradiometric signal due to disturbances of the target structure, e.g., the swaying of branches.
Data Links	
Irradiance Data Link*	A link in the information system, pointing to irradiance data measured by, e.g., a PAR sensor or a sun photometer, and stored as separate radiometric measurement series. Required to explore links between photosynthetic photon flux density, GPP, and F [16].
Uncertainty*	A collection of uncertainty information linked to the traceability chain. Quantifies the uncertainty of various sources of uncertainty with the uncertainty of the retrieved F being the propagated uncertainty [17].
PDFs	
Experimental Design	A document in PDF format describing the experimental design of the study. Useful to raise contextual awareness.
Pictures	
Sampling Environment Picture	Shows the surrounding area to give an impression of influencing factors such as terrain or nearby scene elements leading to adjacency effects.
Sampling setup Picture	Shows the setup of the instrumentation in relation to the target and the solar principal plane.
Sky Picture	Documents the sky conditions. May be used to calculate the cloud cover and the distribution of clouds in the hemisphere observed by irradiance sensors.
Target Picture	Shows the target, ideally imaged from the same viewpoint as the spectral sensor. May be exploited to extract the target homogeneity, particularly if co-registered with the measurement support.
Processing	
Processing Algorithm	Definition of the processing algorithms applied to the data, including version numbers to establish provenance [18].

Table S2. Instruments used to measure F.

Name	range [nm]	FWHM [nm]	sampling interval [nm]	noise level in NEdL or SNR	spatial res. [pixel]	F retrieved at	retrieval methods
<b>non-imaging</b>							
ASD FieldSpec III	350–2500	3	1.4	NEdL 1.1 x 10 <sup>-9</sup> W/cm <sup>2</sup> /n m/sr			3FLD [19,20,9],
Ocean Optics HR2000+ (FluoSpec system)	680–775	0.13				760	SFM [21,22]
Ocean Optics HR2000+ (TriFLEX system)	630–815	0.5	0.09			687, 760	nFLD [23–25]
Ocean Optics HR4000	707–805	0.13	0.02	300 SNR			SVD, FLD [26]; SFM [26–28]
Ocean Optics HR4000	700–800	0.1	0.04			760	SFM [29]
Ocean Optics QE Pro	645–805	0.31	0.155	1000 SNR	/		FLD, 3FLD, iFLD, pFLD, A-SFM [30]
Ocean Optics STS-VIS (SIF-Sys system)	337–823	3		1500 SNR (nominal)		760	FLD [31]
Ocean Optics USB4000	400–1000	1.5					FLD [32]
Ocean Optics USB4000 (HyUAS system)	350–1000	1.5				760	3FLD [33]
<b>Imaging</b>							
HyScreen fluo	670–780	0.25	0.11	300	378	687 760	3FLD, iFLD [34]
SPECIM PS V10E	400–100	3.8	0.63		1392	760	3FLD [35,36]
HyPlant FLUO (airborne)	670–780	0.25 at O2-A 0.23 at O2-B	0.11	240 calculated from lab measurements	384	760	3FLD [37,28], SFM [38], SVD [28,39,40]

APEX (airborne)	375– 2500	0.6–6.3	0.5–8	625 [165]	285	760	3FLD [1]
--------------------	--------------	---------	-------	-----------	-----	-----	----------

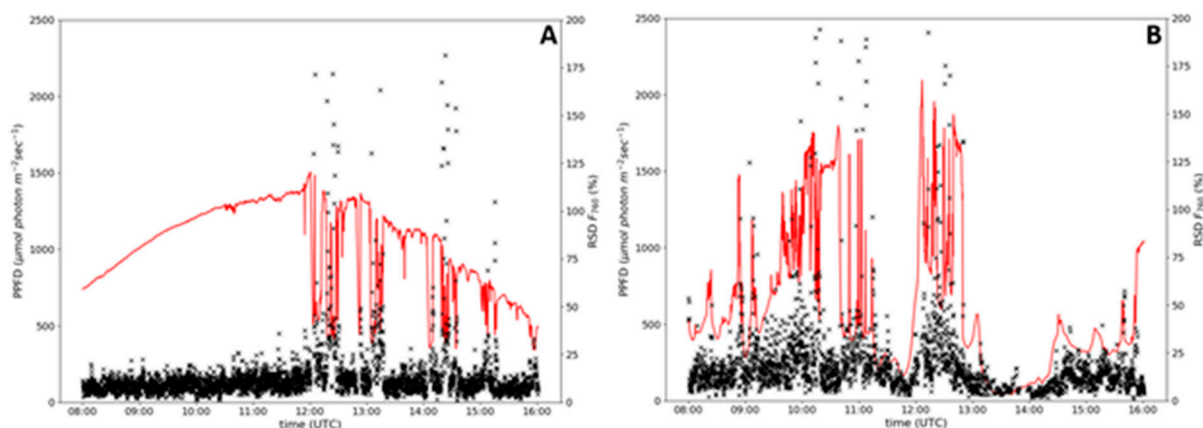


**Figure S1.** Diurnal photosynthetic photon flux density (PPFD; red line) and relative standard deviation of fluorescence at 760 nm ( $F_{760}$ ; black cycles) for a sunny day with few clouds (A) and a cloudy day with strong cloud cover (B). Measurements were taken with a QE Pro over sugar beet on 20.08.2015 (A) and 30.07.2015 (B), Merzenhausen, Germany. The spectroradiometer system has a spectral resolution of 1 nm FWHM (full-width at half maximum), a spectral sampling interval (SI) of 0.3 nm, and a signal-to-noise ratio (SNR) of 1000:1 in a spectral range from 300 to 1000 nm. Measurements were taken every 6–8 seconds.

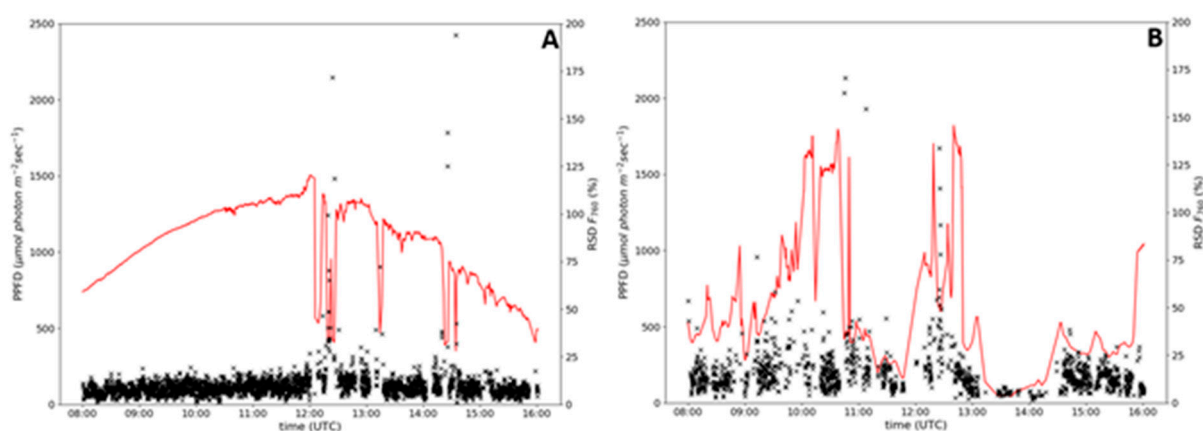


**Figure S2.** Diurnal photosynthetic photon flux density (PPFD; red line) and relative standard deviation of fluorescence at 760 nm ( $F_{760}$ ; black cycles) for a sunny day with few clouds (A) and a cloudy day with strong cloud cover (B) after using a 1% illumination filter. Measurements were taken with a QE Pro over sugar beet on 20.08.2015 (A) and 30.07.2015 (B), Merzenhausen, Germany. The spectroradiometer system has a spectral resolution of 1 nm FWHM (full-width at half maximum), a spectral sampling interval (SI) of 0.3 nm, and a signal-to-noise ratio (SNR) of 1000:1 in a spectral range from 300 to 1000 nm. Measurements were taken every 6–8 seconds.

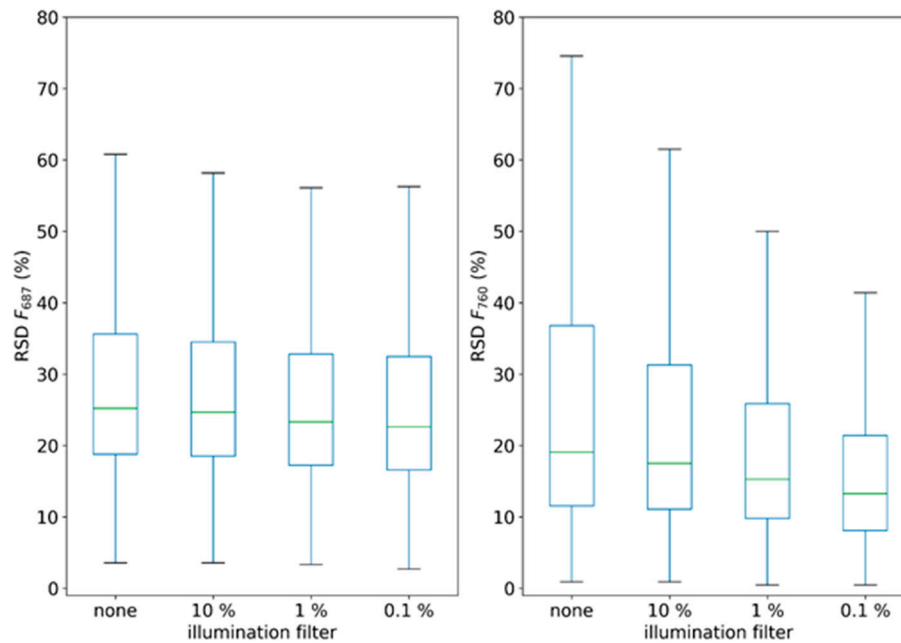


**Figure S3.** Boxplot of the relative standard deviation (RSD) of fluorescence at 760 and 687 nm ( $F_{760}$  and  $F_{687}$ ) for four different illumination quality filters. The dataset was measured over 65 days from June to August 2015 within a sugar beet field in Merzenhausen, Germany. The quality filter labeled “none” does not consider illumination changes between two measurement cycles (6–8 s), the quality filters 10%, 1%, and 0.1% discard samples that show an illumination change of 10, 1, 0.1% between two measurement cycles, respectively. The green bar in the Boxplot shows the median value, the whiskers show the minimum and maximum RSD, the lower box border shows the first quartile, and the upper box border the third quartile.

## References

1. Damm, A.; Guanter, L.; Verhoef, W.; Schläpfer, D.; Garbari, S.; Schaepman, M.E. Impact of varying irradiance on vegetation indices and chlorophyll fluorescence derived from spectroscopy data. *Remote Sens. Environ.* **2015**, *156*, 202–215.
2. Kaiser, J.W.; Schlapfer, D.R.; Brazile, J.; Strobl, P.; Schaepman, M.E.; Itten, K.I. *Assimilation of Heterogeneous Calibration Measurements for the APEX Spectrometer*; Meynart, R., Neeck, S.P., Shimoda, H., Lurie, J.B., Aten, M.L., Eds.; Proc. SPIE 5234, Sensors, Systems, and Next-Generation Satellites VII, 2 February, Barcelona, Spain, **2004**, doi: 10.1117/12.511126.
3. Anderson, K.; Rossini, M.; Pacheco-Labrador, J.; Balzarolo, M.; Mac Arthur, A.; Fava, F.; Julitta, T.; Vescovo, L. Inter-comparison of hemispherical conical reflectance factors (HCRF) measured with four fibre-based spectrometers. *Opt. Express* **2013**, *21*, 605.
4. Pacheco-Labrador, J.; Martín, M.P. Characterization of a field spectroradiometer for unattended vegetation monitoring. Key sensor models and impacts on reflectance. *Sensors* **2015**, *15*, 4154–4175.
5. Hueni, A.; Bialek, A. Cause, Effect, and Correction of Field Spectroradiometer Interchannel Radiometric Steps. *IEEE J. Sel. Top. Appl. Earth Obs. Remote Sens.* **2017**, *10*, 1542–1551.
6. Pacheco-Labrador, J.; Ferrero, A.; Martín, M.P. Characterizing integration time and gray-level-related nonlinearities in a NMOS sensor. *Appl. Opt.* **2014**, *53*, 7778.
7. Daumard, F.; Goulas, Y.; Ounis, A.; Pedrós, R.; Moya, I. Measurement and Correction of Atmospheric Effects at Different Altitudes for Remote Sensing of Sun-Induced Fluorescence in Oxygen Absorption Bands. *IEEE Trans. Geosci. Remote Sens.* **2015**, *53*, 5180–5196.
8. Aasen, H.; Bolten, A. Multi-temporal high-resolution imaging spectroscopy with hyperspectral 2D imagers – From theory to application. *Remote Sens. Environ.* **2018**, *205*, 374–389.

9. Zhao, F.; Li, Y.; Dai, X.; Verhoef, W.; Guo, Y.; Shang, H.; Gu, X.; Huang, Y.; Yu, T.; Huang, J. Simulated impact of sensor field of view and distance on field measurements of bidirectional reflectance factors for row crops. *Remote Sens. Environ.* **2015**, *156*, 129–142.
10. Mac Arthur, A.; MacLellan, C.J.; Malthus, T. The Fields of View and Directional Response Functions of Two Field Spectroradiometers. *IEEE Trans. Geosci. Remote Sens.* **2012**, *50*, 3892–3907.
11. Schaepman-Strub, G.; Schaepman, M.E.; Painter, T.H.; Dangel, S.; Martonchik, J.V. Reflectance quantities in optical remote sensing—definitions and case studies. *Remote Sens. Environ.* **2006**, *103*, 27–42.
12. Balzarolo, M.; Anderson, K.; Nichol, C.; Rossini, M.; Vescovo, L.; Arriga, N.; Wohlfahrt, G.; Calvet, J.-C.; Carrara, A.; Cerasoli, S.; et al. Ground-based optical measurements at European flux sites: A review of methods, instruments and current controversies. *Sensors* **2011**, *11*, 7954–7981.
13. Hueni, A.; Damm, A.; Kneubuehler, M.; Schlapfer, D.; Schaepman, M.E. Field and Airborne Spectroscopy Cross Validation—Some Considerations. *IEEE J. Sel. Top. Appl. Earth Obs. Remote Sens.* **2016**, *10*, 1117–1135.
14. Green, R.O.; Conel, J.E.; Roberts, D.A. Estimation of Aerosol Optical Depth, Pressure Elevation, Water Vapor, and Calculation of Apparent Surface Reflectance from Radiance Measured by the Airborne Visible/Infrared Imaging Spectrometer (AVIRIS) Using a Radiative Transfer Code; Proc. SPIE 1937, Imaging Spectrometry of the Terrestrial Environment, 23 September, Orlando, FL, USA, **1993**; doi: 10.1117/12.157054.
15. Cogliati, S.; Colombo, R.; Celesti, M.; Tagliabue, G.; Rascher, U.; Schickling, A.; Rademske, P.; Alonso, L.; Sabater, N.; Schuettemeyer, D.; et al. Red and Far-Red Fluorescence Emission Retrieval from Airborne High-Resolution Spectra Collected by the Hyplant-Fluo Sensor. In Proceedings of the 2018 IEEE International Geoscience and Remote Sensing Symposium (IGARSS), 22–27 July, Valencia, Spain, 3935–3938.
16. Paul-Limoges, E.; Damm, A.; Hueni, A.; Liebisch, F.; Eugster, W.; Schaepman, M.E.; Buchmann, N. Effect of environmental conditions on sun-induced fluorescence in a mixed forest and a cropland. *Remote Sens. Environ.* **2018**, *219*, 310–323.
17. Woolliams, E.; Hueni, A.; Gorrone, J. Intermediate Uncertainty Analysis for Earth Observation (Instrument Calibration). EMRP-ENV04-D5.2.2\_textbook, European Metrology Research Programme: 129. 2015 Available online: <http://www.emceoc.org/documents/uaeo-int-trg-course-v2.pdf> (accessed on 8 February 2019).
18. Hueni, A.; Lenhard, K.; Baumgartner, A.; Schaepman, M.E. Airborne Prism Experiment Calibration Information System. *IEEE Trans. Geosci. Remote Sens.* **2013**, *51*, 5169–5180.
19. Damm, A.; Guanter, L.; Laurent, V.C.E.; Schaepman, M.E.; Schickling, A.; Rascher, U. FLD-based retrieval of sun-induced chlorophyll fluorescence from medium spectral resolution airborne spectroscopy data. *Remote Sens. Environ.* **2014**, *147*, 256–266.
20. Damm, A.; Erler, A.; Hillen, W.; Meroni, M.; Schaepman, M.E.; Verhoef, W.; Rascher, U. Modeling the impact of spectral sensor configurations on the FLD retrieval accuracy of sun-induced chlorophyll fluorescence. *Remote Sens. Environ.* **2011**, *115*, 1882–1892.
21. Yang, X.; Tang, J.; Mustard, J.F.; Lee, J.-E.; Rossini, M.; Joiner, J.; Munger, J.W.; Kornfeld, A.; Richardson, A.D. Solar-induced chlorophyll fluorescence that correlates with canopy photosynthesis on diurnal and seasonal scales in a temperate deciduous forest. *Geophys. Res. Lett.* **2015**, *42*, 2977–2987.
22. Yang, H.; Yang, X.; Zhang, Y.; Heskell, M.A.; Lu, X.; Munger, J.W.; Sun, S.; Tang, J. Chlorophyll fluorescence tracks seasonal variations of photosynthesis from leaf to canopy in a temperate forest. *Glob. Chang. Biol.* **2017**, *23*, 2874–2886.
23. Daumard, F.; Champagne, S.; Fournier, A.; Goulas, Y.; Ounis, A.; Hanocq, J.F.; Moya, I. A Field Platform for Continuous Measurement of Canopy Fluorescence. *IEEE Trans. Geosci. Remote Sens.* **2010**, *48*, 3358–3368.
24. Goulas, Y.; Fournier, A.; Daumard, F.; Champagne, S.; Ounis, A.; Marloie, O.; Moya, I. Gross Primary Production of a Wheat Canopy Relates Stronger to Far Red Than to Red Solar-Induced Chlorophyll Fluorescence. *Remote Sens.* **2017**, *9*, 97.
25. Daumard, F.; Goulas, Y.; Champagne, S.; Fournier, A.; Ounis, A.; Olioso, A.; Moya, I. Continuous Monitoring of Canopy Level Sun-Induced Chlorophyll Fluorescence During the Growth of a Sorghum Field. *IEEE Trans. Geosci. Remote Sens.* **2012**, *50*, 4292–4300.

26. Guanter, L.; Rossini, M.; Colombo, R.; Meroni, M.; Frankenberg, C.; Lee, J.-E.; Joiner, J. Using field spectroscopy to assess the potential of statistical approaches for the retrieval of sun-induced chlorophyll fluorescence from ground and space. *Remote Sens. Environ.* **2013**, *133*, 52–61.
27. Migliavacca, M.; Perez-Priego, O.; Rossini, M.; El-Madany, T.S.; Moreno, G.; van der Tol, C.; Rascher, U.; Berninger, A.; Bessenbacher, V.; Burkart, A.; et al. Plant functional traits and canopy structure control the relationship between photosynthetic CO<sub>2</sub> uptake and far-red sun-induced fluorescence in a Mediterranean grassland under different nutrient availability. *New Phytol.* **2017**, *214*, 1078–1091.
28. Rossini, M.; Nedbal, L.; Guanter, L.; Ač, A.; Alonso, L.; Burkart, A.; Cogliati, S.; Colombo, R.; Damm, A.; Drusch, M.; et al. Red and far red Sun-induced chlorophyll fluorescence as a measure of plant photosynthesis. *Geophys. Res. Lett.* **2015**, *42*, 1632–1639.
29. Cogliati, S.; Rossini, M.; Julitta, T.; Meroni, M.; Schickling, A.; Burkart, A.; Pinto, F.; Rascher, U.; Colombo, R. Continuous and long-term measurements of reflectance and sun-induced chlorophyll fluorescence by using novel automated field spectroscopy systems. *Remote Sens. Environ.* **2015**, *164*, 270–281.
30. Liu, L.; Liu, X.; Hu, J.; Guan, L. Assessing the wavelength-dependent ability of solar-induced chlorophyll fluorescence to estimate the GPP of winter wheat at the canopy level. *Int. J. Remote Sens.* **2017**, *38*, 4396–4417.
31. Burkart, A.; Schickling, A.; Mateo, M.P.C.; Wrobel, T.J.; Rossini, M.; Cogliati, S.; Julitta, T.; Rascher, U. A Method for Uncertainty Assessment of Passive Sun-Induced Chlorophyll Fluorescence Retrieval Using an Infrared Reference Light. *IEEE Sens. J.* **2015**, *15*, 4603–4611.
32. Cheng, Y.-B.; Middleton, E.M.; Zhang, Q.; Huemmrich, K.F.; Campbell, P.K.E.; Corp, L.A.; Cook, B.D.; Kustas, W.P.; Daughtry, C.S. Integrating Solar Induced Fluorescence and the Photochemical Reflectance Index for Estimating Gross Primary Production in a Cornfield. *Remote Sens.* **2013**, *5*, 6857–6879.
33. Garzonio, R.; Mauro, B.D.; Colombo, R.; Cogliati, S. Surface Reflectance and Sun-Induced Fluorescence Spectroscopy Measurements Using a Small Hyperspectral UAS. *Remote Sens.* **2017**, *9*, 472.
34. Cendrero-Mateo, M.P. HyScreen: Hyperspectral Ground Imaging System for reflectance and fluorescence. In Proceedings of the Remote Sensing of Fluorescence, Photosynthesis and Vegetation Status, Frascati, Italy, 17–19 January, Frascati, Italy, **2017**.
35. Pinto, F.; Damm, A.; Schickling, A.; Panigada, C.; Cogliati, S.; Müller-Linow, M.; Balvora, A.; Rascher, U. Sun-induced chlorophyll fluorescence from high-resolution imaging spectroscopy data to quantify spatio-temporal patterns of photosynthetic function in crop canopies: Sun-induced fluorescence in crop canopies. *Plant Cell Environ.* **2016**, *39*, 1500–1512.
36. Pinto, F.; Müller-Linow, M.; Schickling, A.; Cendrero-Mateo, M.; Balvora, A.; Rascher, U. Multiangular Observation of Canopy Sun-Induced Chlorophyll Fluorescence by Combining Imaging Spectroscopy and Stereoscopia. *Remote Sens.* **2017**, *9*, 415.
37. Rascher, U.; Alonso, L.; Burkart, A.; Cilia, C.; Cogliati, S.; Colombo, R.; Damm, A.; Drusch, M.; Guanter, L.; Hanus, J.; et al. Sun-induced fluorescence—A new probe of photosynthesis: First maps from the imaging spectrometer HyPlant. *Glob. Chang. Biol.* **2015**, *21*, 4673–4684.
38. Wieneke, S.; Ahrends, H.; Damm, A.; Pinto, F.; Stadler, A.; Rossini, M.; Rascher, U. Airborne based spectroscopy of red and far-red sun-induced chlorophyll fluorescence: Implications for improved estimates of gross primary productivity. *Remote Sens. Environ.* **2016**, *184*, 654–667.
39. Middleton, E.M.; Rascher, U.; Corp, L.A.; Huemmrich, K.F.; Cook, B.D.; Noormets, A.; Schickling, A.; Pinto, F.; Alonso, L.; Damm, A.; et al. The 2013 FLEX—US Airborne Campaign at the Parker Tract Loblolly Pine Plantation in North Carolina, USA. *Remote Sens.* **2017**, *9*, 612.
40. Colombo, R.; Celesti, M.; Bianchi, R.; Campbell, P.K.E.; Cogliati, S.; Cook, B.D.; Corp, L.A.; Damm, A.; Domec, J.-C.; Guanter, L.; et al. Variability of sun-induced chlorophyll fluorescence according to stand age-related processes in a managed loblolly pine forest. *Glob. Chang. Biol.* **2018**, *24*, 2980–2996.